CHEMISTRY
A EUROPEAN JOURNAL

COMMUNICATION

DOI: 10.1002/chem.201300418

Construction of Long-Wavelength Fluorescein Analogues and Their Application as Fluorescent Probes

Xiaoqing Xiong,[a] Fengling Song,*[a] Gengwen Chen,[a] Wen Sun,[a] Jingyun Wang,[b] Pan Gao,[b] Yukang Zhang,[a] Bo Qiao,[a] Wenfang Li,[b] Shiguo Sun,[a] Jiangli Fan,[a] and Xiaojun Peng*[a]

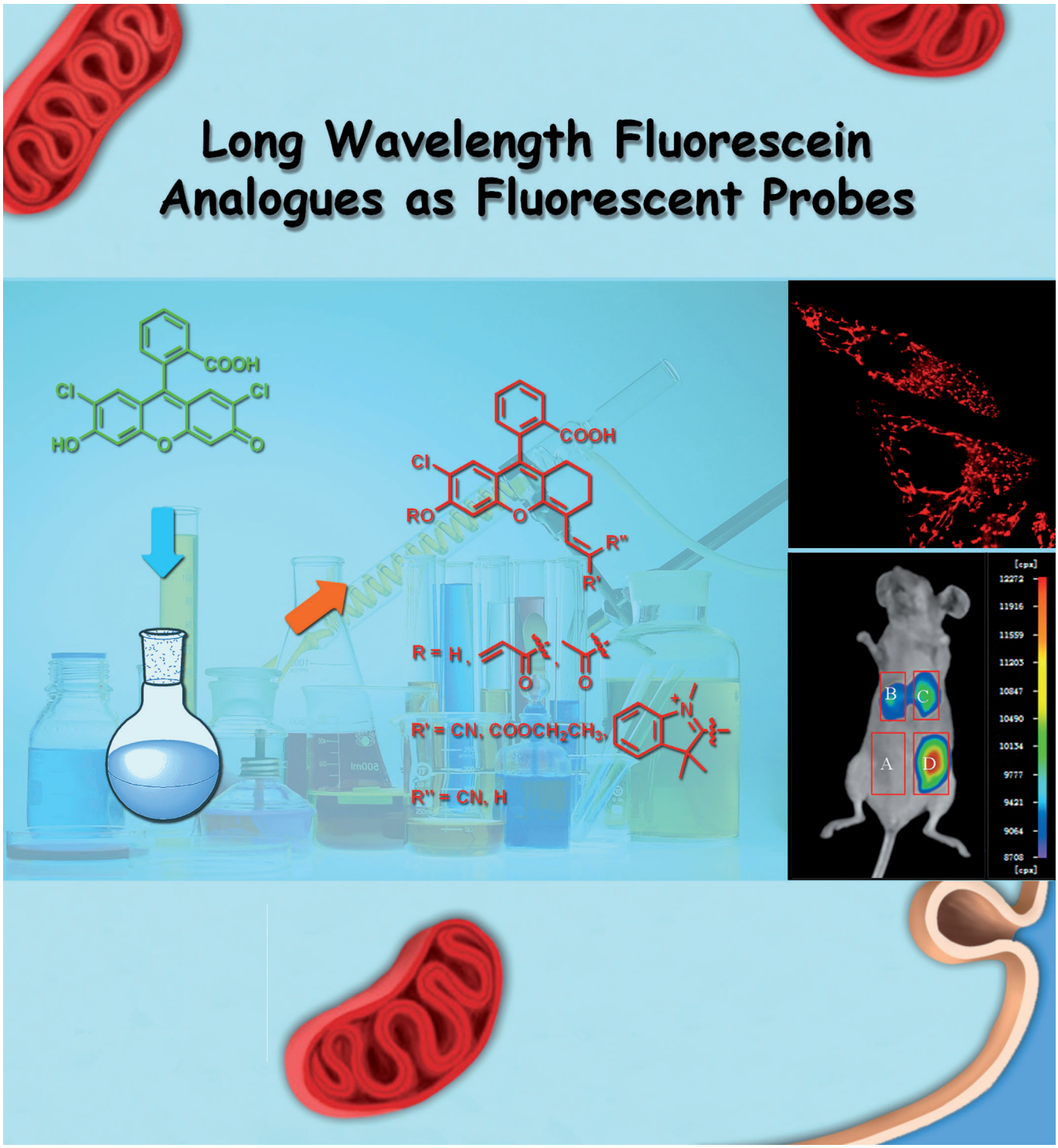

Fluorescence imaging is one of the most powerful techniques for monitoring biomolecules in living systems.[1] Compared with fluorescent imaging in the visible region, biological imaging in red and near-infrared (NIR) region is favourable due to its minimum photodamage, deep tissue penetration, and minimum background autofluorescence caused by biomolecules in living systems.[2] Therefore, chromophores with emission in red or near-infrared region have been paid increasing attention in recent years.

The most widely employed NIR fluorophores are cyanine dyes, especially Cy5.5 and Cy7.[3] However, to the best of our knowledge, this kind of dye suffers from severe disadvantages, like bad photostability and low fluorescence quantum yield. Therefore, many groups have tried to develop new fluorophores based on rhodamine[4] and BODIPY, the spectra of which can extend to the red and even NIR region through modification.[5] For example, Nagano and colleagues designed and synthesised a novel NIR Si–rhodamine fluorescence probe MMSiR.[4a] They have developed a series of novel NIR wavelength-excited fluorescent dyes, SiR-NIRs, by modifying the Si–rhodamine scaffold.[4b,6] They have also developed 2-Me TeR as a reversible NIR fluorescence probe.[4c] Other groups have also constructed red-emissive or NIR BODIPY dyes.[5,7] However, very few red or NIR fluorescein derivatives have been constructed.[8,9] As a matter of fact, fluoresceins have predominant photostability, which makes them suitable for biological application.

Fluorescein dyes have good photochemical properties, such as high molar extinction coefficients, large fluorescence quantum yields and tolerance to photobleaching.[10] Significantly, alkylation of the hydroxyl of fluorescein can easily tune the fluorescence property. So far, the hydroxyl-alkylation fluoresceins have become an effective platform for construction of fluorescence turn-on sensors. Many probes for a diverse array of targets including hydrogen peroxide,[11] peroxynitrite,[12] superoxide radical,[13] and cysteine[14] have been reported based on the unique hydroxyl alkylation principle. However, these probes' absorption and emission wavelengths are in the visible region. To make full use of the hydroxyl alkylation principle, it is highly desirable to develop stable fluorescein analogues with absorption and emission in the red or NIR region.

[a] X. Xiong, Prof. F. Song, Dr. G. Chen, W. Sun, Y. Zhang, B. Qiao, Dr. S. Sun, Dr. J. Fan, Prof. X. Peng
State Key Laboratory of Fine Chemicals
Dalian University of Technology, 2 Linggong Road
Dalian 116025 (P.R. China)
E-mail: songfl@dlut.edu.cn
pengxj@dlut.edu.cn

[b] J. Wang, P. Gao, W. Li
School of Life Science & Biotechnology
Dalian University of Technology, 2 Linggong Road
Dalian 116025 (P.R. China)

Supporting information for this article is available on the WWW under http://dx.doi.org/10.1002/chem.201300418.

Herein, we present the synthesis of a new 2′,7′-dichlorofluorescein (DCF) analogue with red emission. The intermediate aldehyde **3** was synthesised by the Vilsmeier reaction without further purification and was used to prepare the subsequent products by Knoevenagel condensation (Scheme 1). We expect that this design strategy can be extended to the development of a wide variety of long-wavelength functional dyes and then to further applications in biological studies.

We first tested the optical properties of dye **4** in different solvents, such as H_2O, ethanol, DMSO and so on (Table S1 in the Supporting Information). The absorption and emission spectra of **4** in DMSO are illustrated in Figure 1. Dye **4**

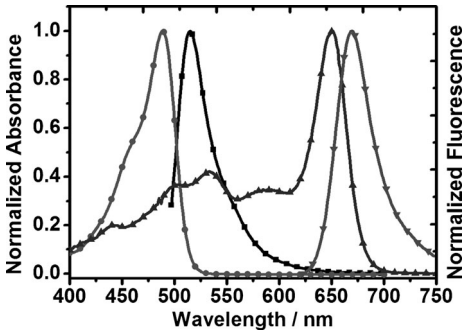

Figure 1. The normalised absorbance (●) and fluorescence (■) spectra of DCF (2.0 μM in water, $\lambda_{ex}=490$ nm). The normalised absorbance (▲) and fluorescence (▼) spectra of **4** (2.0 μM in DMSO, $\lambda_{ex}=620$ nm).

exhibited a high extinction coefficient (62505 $M^{-1}cm^{-1}$) and with full width at half maximum (40 nm) in DMSO. Compared with traditional DCF, the absorption and emission spectra of **4** can extend to the NIR range. The fluorescence quantum yield of the NIR fluorescein analogue **4** was measured to be as high as 0.55 (rhodamine B was used as a standard: $\Phi=0.97$ in ethanol).

To rationalise the optical properties of the new functional dye **4**, representative optimised structures and molecular orbital plots (LUMO and HOMO) were obtained by density functional theory (DFT) calculations with the B3LYP exchange functional employing 6-31G(d,p) basis sets with a suite of Gaussian 09 programs (Figure 2). The π electrons on the HOMO of **4** are mainly located on the whole π-conjugated 7,8-dihydro-6*H*-xanthene-dicyanovinyl framework (including the O and Cl atoms), but electrons of the LUMO are mostly positioned at the centre of the conjugated 7,8-dihydro-6*H*-xanthene-vinyl bridge (Figure 2). Therefore, the DFT calculation results (Tables S5–S7 in the Supporting Information) are consistent with the absorption and emission spectroscopic data of **4** (Table S1 in the Supporting Information). In addition, time-dependent DFT (TDDFT) calculations indicated that the excitation HOMO–LUMO energy gap between the S_0 state and the S_1 excited state of **4** (2.6616, 1.9924 eV based on the optimised S_0 or S_1 state geometry) is calculated by DFT calculation (Tables S5–S7 in the Supporting Information).

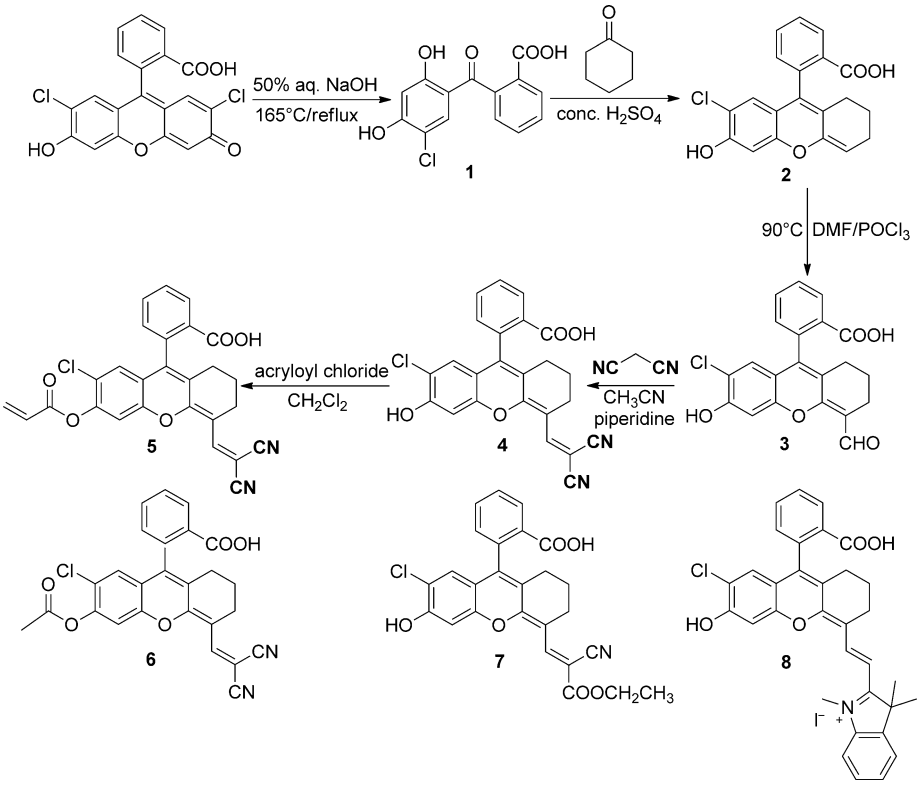

Scheme 1. The synthetic routes to DCF analogue **4** and the derivatives **5**, **6**, **7** and **8**.

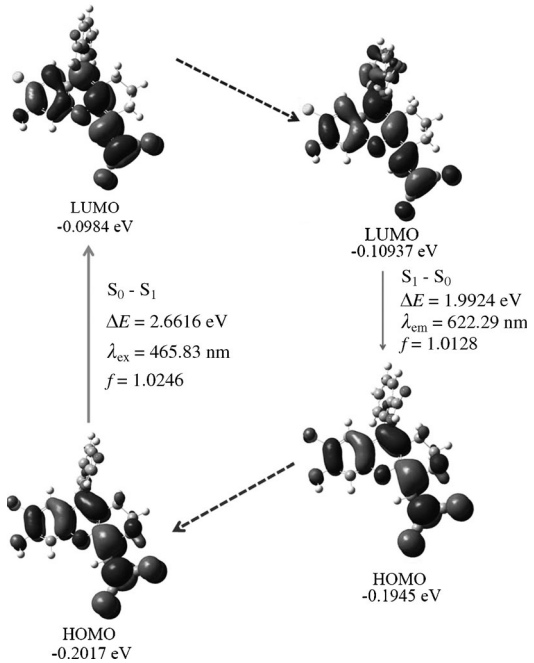

Figure 2. Frontier molecular orbital plots of **4** in water; it is involved in the vertical excitation (UV/Vis absorption, left column) and emission (right column). The vertical-excitation-related calculations are based on the optimised geometry of the ground state (S_0), and the emission-related calculations are based on the optimised geometry of the excited state (S_1). Excited and radioactive processes are marked as solid lines and the non-radiative processes are marked by dotted lines.

The photostability is of great importance for long-wavelength dyes. The stability measurement of **4** was carried out in comparison with a commercial NIR dye (Mitotracker Deep Red). Dye **4** was found to be reasonably stable (Figure S1 in the Supporting Information). The fluorescence spectra of **4** at various pH values (the pH ranges from 3.28 to 12.58) are recorded in Figure S2a (in the Supporting Information). The fluorescence was significantly enhanced with pH increasing together with a 63-fold increase of emission intensity. As shown in Figure S2b (in the Supporting Information), the changes in the fluorescence intensity as a function of pH yielded a pK_a of 6.41. The absorption spectrum appeared to have an altered ratio (Figure S3 in the Supporting Information). It is well-known that the emission wavelength of a D-π-A chromophore is sensitive to the polarity of the solvent.[15] Thus, we analysed the emission changes of dye **4** in water/1,4-dioxane system with different polarity (Figure S4 in the Supporting Information). To our delight, the new dye **4** is not sensitive to polarity. This solvent-polarity independent emission wavelength will make this dye ideal for further construction of fluorescent probes.

In order to explore the biological application of fluorophore **4**, we utilised it to stain HeLa cells; the results showed that **4** does not performs well (Figure 3). Although it can enter the cells, it does not exhibit obvious organelle staining. We presume that the possible reason is that the molecule contains more hydrophilic groups (such as hydroxyl, cyan, carboxyl); these groups may reduce the membrane permeability. Therefore, we decided to broaden the new fluorophore's application and improve its lipid solubility. Based on the above two requirements, we designed and syn-

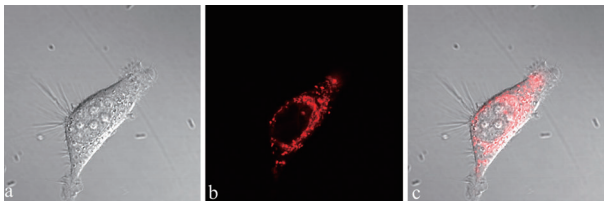

Figure 3. Confocal fluorescence images of HeLa cells incubated with **4** (20 μM) at 37 °C. After 150 min incubation: a) bright-field image; b) fluorescent image with excitation at 635 nm for red emission of **4** (640 ± 20 nm); c) overlay of (a) and (b).

thesised the control substances **5**, **6**, **7**, **8**, the structures of which are similar to dye **4** (Scheme 1). We investigated the optical properties of these compounds, and the results are summarised in Tables S2–S4 and Figures S5, S6 in the Supporting Information. Compound **5** shows almost no fluorescence in various solvents; weak background fluorescence is useful for application as a fluorescent probe. From the absorption and emission spectra data in different solvents, it was observed that the spectral changes of **6** and **7** are very similar to **4**. However, to our surprise, the fluorescence of dye **6**, the hydroxyl of which was modified by acetylation, was not completely quenched.

As illustrated in Figure 4, to estimate the potential use of these derivatives for biological imaging, MCF-7 cells (breast cancer cell line) were incubated with **6** (20 μM) and **7** (20 μM) at 37 °C for 120 min. As shown in Figure 4 a–c and d–f, both dyes proved to be membrane permeant. Their fluorescence was detected in the cytoplasmic rather than nuclear regions. Based on morphological grounds, these regions were judged to be the mitochondria.

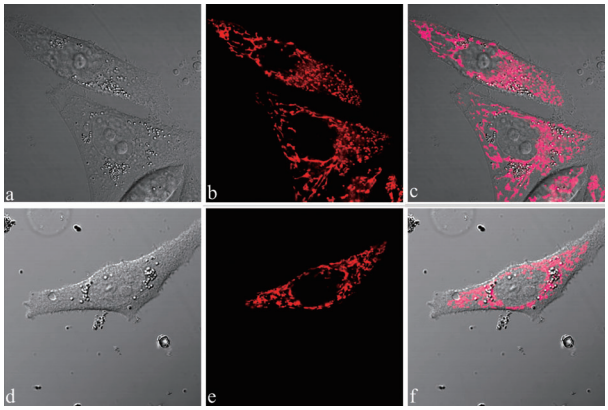

Figure 4. Confocal fluorescence images of MCF-7 cells incubated with **6** (20 μM, top row) and **7** (20 μM, bottom row) at 37 °C. After 2.0 h incubation: a), d) bright-field images; b), e) fluorescent images with excitation at 488 nm for red emission of **6** and **7** (590 ± 50 nm); c), f) overlays of (a) and (b), and (d) and (e), respectively.

To further investigate the subcellular localisation of compound **6** and **7**, organelle-specific fluorescent dye (MitoTracker Green FM) was employed for colocalisation studies. Staining experiments of **6** and **7** were performed with MCF-7 cells and show that both **6** and **7** colocalised in the mitochondria (Figure 5). With different incubation times (MitoTracker Green FM, 30 min; **6** and **7**, 120 min), both were found to localise selectively in mitochondria with a bright fluorescent signal. The Pearson's sample correlation factors (R_r) of colocalisation with MitoTracker Green FM were found to be 97 and 93 % in MCF-7 cells, for **6** and **7**, respectively. Mitochondria supply the cells' energy, and are very important but sensitive and variable organelles. So when mitochondria are simulated by external factors, their morphology, size, number and distribution can change significantly.[16] Besides, mitochondria are crucially involved in a variety of pathologies, from Alzheimer's disease to cancers and diabetes.[17] Mitochondrial morphological analysis, therefore, attracts immense interest.

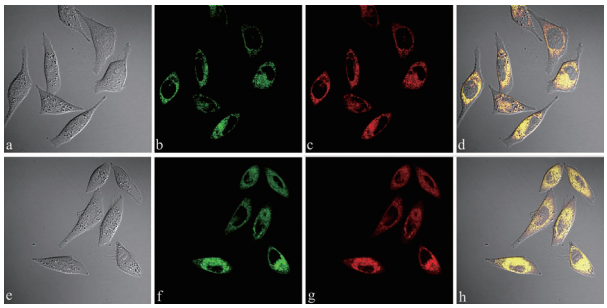

Figure 5. Confocal images of **6** (20 μM, top row) and **7** (20 μM, bottom row) at 37 °C with mitochondrial-specific dye in MCF-7 cells: a) bright-field image; b) fluorescent image of MCF-7 cells stained with MitoTracker Green FM; c) fluorescent image of MCF-7 cells stained with **6**; d) merged image of (a), (b) and (c); e) bright-field image; f) fluorescent image of MCF-7 cells stained with MitoTracker Green FM; g) fluorescent image of MCF-7 cells stained with **7**; h) merged image of (e), (f) and (g), excited at 488 nm for MitoTracker Green FM, green emission (520 ± 20 nm); excited at 488 nm for **6** and **7**, red emission (590 ± 50 nm).

Figure 6, shows different damaged mitochondrial forms. Figure 6 h and k represent hollow spheres of extremely swollen mitochondria; in Figure 6 g and j the mitochondria are less swollen and appear as solid granules. The two dyes can be used to monitor different degrees of mitochondrial damage. The above results show that these derivatives have good membrane permeability, and will provide a good platform for further exploring mitochondrial fluorescent probes.

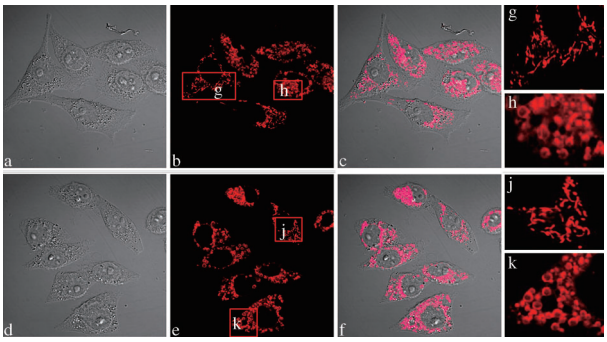

Figure 6. Confocal fluorescence images of MCF-7 cells incubated with 5 μM of dye **6** (top row) or **7** (bottom row). After incubation for 10 h: a), d) Bright-field images; b), e) various damaged mitochondrial forms; c), f) cells stained with **6** and **7**, respectively; g), h) magnification of marked areas in (b); j), k) magnification of marked areas in (e).

The probable reason for the good mitochondrial staining of dyes **6** and **7** is that they are lipophilic weak acids. According to the reported literatures,[18] lipophilic weak acids comprise equilibrium mixtures of lipophilic-free acids and their more hydrophilic salts under physiological condition. The entry of probes into cells mainly depends on their lipophilicity, which is modelled by their water/octanol partition

coefficient ($\log P$) values.[19] On the basis of simulations (ChemDraw) the $\log P$ values for **6** and **7** were 3.57 and 3.64, respectively. Specifying mitochondria accumulation is assigned numerically by the following criteria: $+5 > \log P > 0$.[18] This can explain why the new dyes can accumulate in the mitochondria.

Equilibrium is re-established between free acids and hydrophilic salts in the aqueous environment in living cells. The equilibrium is dependent on the pH of the compartment. This effect controls the probes' accumulation in the mitochondria, because the internal pH of mitochondria (pH $\approx$8.0) is higher than that of the cytosol (pH$\approx$7.5).[20] This somewhat alkaline environment results in the decrease of the relative concentration of lipophilic free acid, but the concentration of the ionised species is relatively increased. Then, the corresponding weak acids become more hydrophilic, and these anions will be less membrane permeant and consequently accumulate inside the mitochondria. Based on the literature,[21] the process for the accumulation of **7** in mitochondria is illustrated in Scheme 2. The accumulation of **6** can be attributed to the same mechanism.

For dye **8** (Figures S5 and S6 in the Supporting Information), the absorption and emission spectra can extend to the NIR region. We utilised dye **8** in biological tests to expand its applications. The results show that dye **8** can also stain mitochondria (Figure 7). This can be explained in terms of the positive charge of dye **8**. As with the common mitochondrial dyes, in order to balance the potential of the mitochondrial membrane, the molecule can enter the mitochondria.

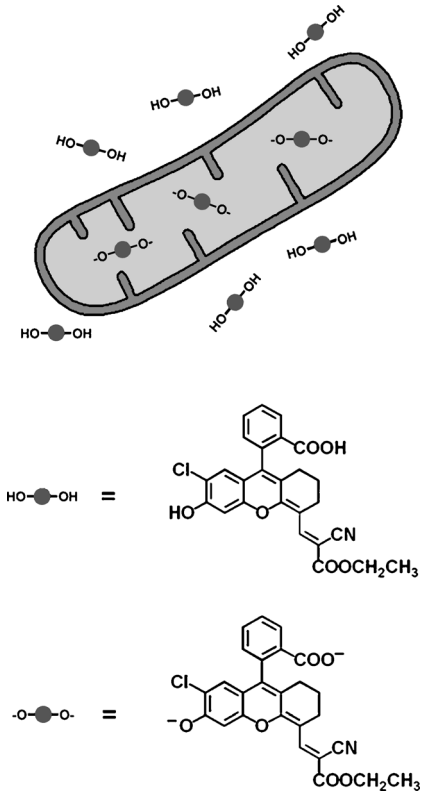

Scheme 2. Schematic illustration of the mechanism for ion-trapping of **7**.

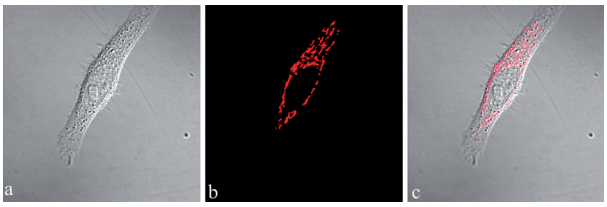

Figure 7. Confocal fluorescence images of HeLa cells incubated with **8** (5 μM) at 37 °C. After 30 min incubation: a) bright-field image; b) fluorescent image with excitation at 635 nm for **8**, red emission (705 ± 50 nm); c) overlay of (a) and (b).

As illustrated in Figure S7 (in the Supporting Information), the colocalisation results suggest that **8** can selectively stain mitochondria in living cells.

Compared with the above-mentioned compounds, dye **5** exhibited almost no fluorescence in different solvents; so the drastic difference in the fluorescence intensity between compound **5** and **4** suggests that **5** can be used as a fluorescent turn-on probe. Recently, Chen's group constructed a fluorescence turn-on sensor for cysteine.[14a] The construction mechanism was employed in our case. Furthermore, to test the robust nature of the approach for novel NIR fluorescein analogues, we utilised the nonfluorescent dye **5** as a new NIR fluorescent turn-on thiol sensor.

Upon addition of cysteine (Cys), homocysteine (Hcy) and glutathione (GSH) to a solution of probe **5**, the fluorescence intensity of the detection system was recorded. The fluorescence intensity increased rapidly with prolonged reaction times, and the reaction of **5** with Cys was nearly complete within 10 min (Figure 8). At the same time, the free probe **5** exhibited no noticeable changes in solution. A similar fluorescence increase was observed for Hcy and GSH, but both

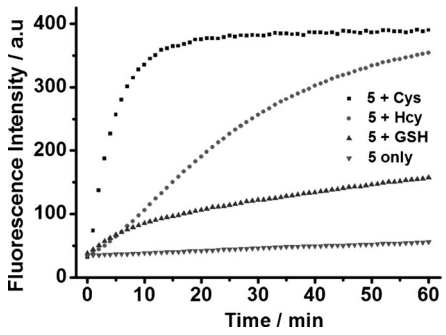

Figure 8. Time course of the fluorescence response (λ_{em} = 650 nm) of probe **5** (5.0 μM) in aqueous solution (40 mM HEPES buffer, pH 7.37) in the presence of 34 equiv Cys, Hcy or GSH, with excitation at 620 nm.

took more than 60 min to reach the maximal intensity. Therefore, to obtain highly sensitive and reproducible results, all experiments were completer within 10 min.

The typical biological thiol, Cys, was examined by the sensing response of probe **5**. After the immediate addition of Cys, the emission colour of probe **5** changed to red (Figure S8 in the Supporting Information). Free **5** is weakly fluorescent perhaps because the acryloyl substituent of **5** re-

duces the electron-donating ability of the oxygen atom and thus forbids the formation of the zwitterionic resonance form. But upon addition of Cys (26 equiv), the fluorescence emission at 650 nm increased about 20-fold within 10 min (Figure S8 in the Supporting Information). The fluorescence intensity of **5** at 650 nm shows a good linear relationship with the concentration of Cys ranging from 0 to 40 μM (Figure S9 in the Supporting Information), and the detection limit for Cys is 0.0309 μM. Increasing the amount of Cys (0–130 μM) added to a solution of probe **5** (5.0 μM) caused the absorption bands of **5** at 474 and 520 nm to gradually decrease, whereas new absorption bands at 576 and 625 nm appeared with a distinct isosbestic point at 525 nm; this resulted in an apparent colour change from red to hyacinthine (Figure 9). This shows that **5** can allow colorimetric detection of Cys with the naked-eye. The combination of the low detection limit and the large fluorescence dynamic range indicates that the probe is highly sensitive to Cys.

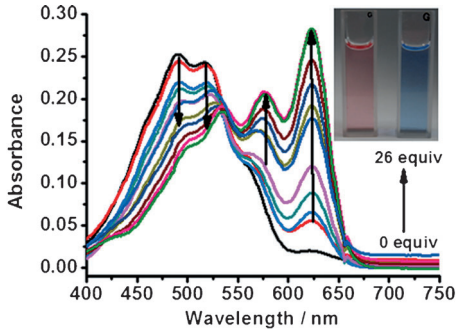

Figure 9. Absorption spectral changes of **5** (5.0 μM in DMSO/HEPES buffer, 7:3) after incubation with different concentrations of cysteine (0, 0.66, 1.32, 2.0, 4.0, 8.0, 10, 14, 18, 22 and 26 equiv). Each spectrum was recorded after 10 min. Inset: probe **5** (5.0 μM) in the absence of Cys (left) and in the presence of 130 μM Cys (right).

The above spectral studies and the sensing response of the probe to Cys indicate that most probably a new compound is formed. So we conducted further experiments to corroborate this. The plausible reaction mechanism for the formation **10** and **4** is proposed in Scheme 3. Mass spectrometry analysis showed the formation of **4** and a cyclised product **10** was obtained from the reaction of **5** with Cys. The peak at 430.0 corresponding to the fluorescent **4** and another peak at 174.0 corresponding to the cyclisation product **10** were clearly observed (Figure S10 in the Supporting Information).

To investigate its selectivity, probe **5** (5.0 μM) was treated with various biologically relevant analytes (such as representative amino acids, metal ions, anions) and monitored by absorption and emission spectroscopy (Figures S11–S16 in the Supporting Information). No noticeable changes in the absorption were observed upon addition of amino acids (alanine, valine, leucine, proline, tyrosine, asparamide and taurine), metal ions (Cd^{2+}, Mg^{2+}, Pt^{2+}, K^{+}, Cr^{3+}, Cu^{2+}, Al^{3+}, Mn^{2+}, Zn^{2+}, Fe^{3+}, Na^{+}, Pd^{2+}, Ca^{2+}, Ag^{+}, Hg^{2+}, NH_4^{+}, Ni^{2+}), and anions (Br^{-}, Ac^{-}, NO_3^{-}, Cl^{-}, ClO_4^{-}, ClO^{-}, CO_3^{2-}, I^{-}, $H_2PO_4^{-}$, HPO_4^{2-}, HCO_3^{-}).

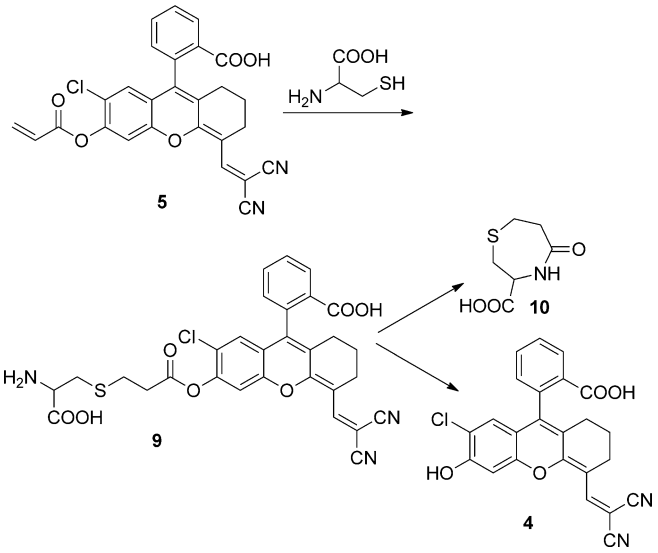

Scheme 3. A plausible mechanism for the reaction between **5** and Cys.

To further establish the utility of **5** for the determination of Cys in a biological sample, we evaluated **5** (50 μM) with commercially available newborn-calf serum (Figure S17 in the Supporting Information). The detection of Cys was achieved successfully in the samples. An excellent linear correlation between the added Cys concentrations and the fluorescence emission responses at $\lambda_{em}=650$ nm was observed in the serum (Figure S18 in the Supporting Information). The fluorescence intensity response in serum was lower than that observed with the detection system used in Figures S8 and S9 in the Supporting Information. However, these data show that physiologically relevant sensitivity and limits of detection can be obtained in detecting Cys in blood plasma.

To assess permeability and ability to monitor thiols in living cells, confocal microscopy experiments were carried out. When MCF-7 cells were incubated with **5** (20 μM) bright fluorescence was exhibited inside the cells (Figure 10b). There was no intracellular background fluores-

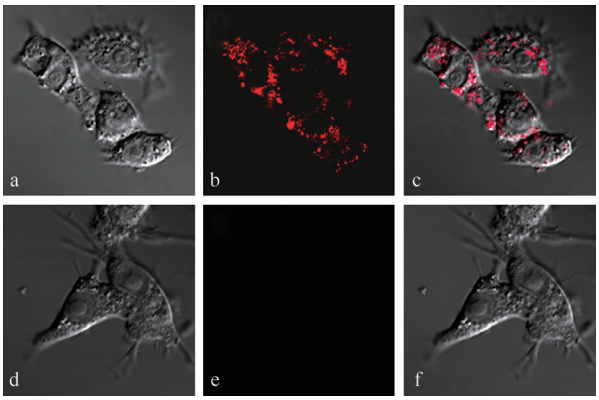

Figure 10. Fluorescence images of MCF-7 cells incubated with (a, b) or without (d, e) **5** (20 μM) at 37 °C. After 90 min incubation: a) bright-field image; b) fluorescent image with excitation at 635 nm; c) overlay of (a) and (b); d) bright-field image; e) fluorescent image with excitation at 635 nm, no fluorescence was observed; f) overlay of (d) and (e).

cence in untreated control cells (Figure 10e). This confirmed that **5** could be used to monitor thiols in living cells. To further test the robust nature of this probe, we examined its application for visualising Cys in living animals. Different concentrations of probe **5** (0, 10, 20 and 50 μM) in 4-(2-hydroxyethyl)-1-piperazineethanesulfonic acid (0.1 mL, 40 mM HEPES buffer, pH 7.37) were injected into mice. Different fluorescence intensities were observed after 10 min, whereas no fluorescence was noted in uninjected regions (Figure 11). The results show that probe **5** also can be exploited for the development of NIR fluorescent sensors for in vivo imaging applications.

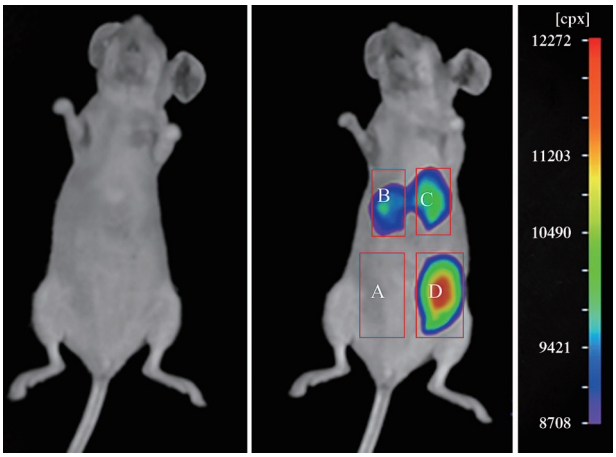

Figure 11. Fluorescent images of mice (pseudocolour) without probe **5** (left) and with injection of different concentrations of probe **5** (right) in HEPES (0.1 mL; 40 mM buffer, pH 7.37). A) 0 μM, B) 10 μM, C) 20 μM, D) 50 μM. Images were taken after incubation for 10 min.

In summary, we have successfully developed a new NIR 2′,7′-dichlorofluorescein analogue **4**, which exhibits high quantum yield, an excellent photostability and cellular permeability. All of these properties are very desirable for NIR fluorophores. Through modification, it was found that the derivatives **6**, **7**, **8** can localise in mitochondria specifically. Moreover, we have demonstrated that the approach can be easily employed to develop NIR thiol fluorescent sensor **5**, which can be used to colorimetrically detect Cys, in vitro. The NIR thiol sensor can be utilised in biological imaging applications. We anticipate that such red-emissive DCF analogues can be very useful as a fluorescence sensing platform.

Experimental Section

Materials and instruments: Common reagents used in the experiments were all of analytical grade. Cyclohexanone, $POCl_3$ and DMF were purchased from Tianjin Bodi Co., Ltd. Et_3N was purchased from Tianjin Damao Chemical Reagent. Malononitrile, acryloyl chloride, acetic anhydride, ethyl cyanoacetate and 2-methyl benzothiazole were purchased from Alading. Cys, Hcy were purchased from Solarbio. GSH was purchased from Tokyo Chemical Industry Co., Ltd. 2′,7′-Dichlorofluorescein-6-carboxylic acid was synthesised according to the literature.[22] Rhodamine B was purchased from Tianjin Fine Chemicals Development Centre. ^1H and ^{13}C NMR spectra were recorded on a Varian Inova-400 spectrometer with chemical shifts reported as ppm (in DMSO or methanol, TMS as internal standard). The following abbreviations are used to indicate the multiplicities: s, singlet; d, doublet; t, triplet; q, quartet; m, multiple; br, broad. Mass spectrometric data were obtained on a Q-TOF Micro mass spectrometer. UV–visible spectra were collected on a Perkin–Elmer Lambda 35 UV/Vis spectrophotometer. Fluorescence measurements were performed on a Varian Cary Eclipse fluorescence spectrophotometer (serial No.: FL1109M018).

Photostability experiment: Compound **4** and Mitotracker Deep Red were dissolved in aqueous solution (DMSO/40 mM HEPES buffer, 7:3, pH 7.37) at a concentration of 2.0 μM. These solutions were irradiated under a 500 W iodine-tungsten lamp for 250 min at a distance of 30 cm away from the lamp. A saturated sodium nitrite aqueous solution was placed between the samples and the lamp as a light filter (to cut off wavelengths shorter than 400 nm) and heat filter.

Calculating pK_a: Dye **4** (15 μM) was dissolved in phosphate-buffered saline (PBS, 50 mL). Then the solution was divided into two equivalent parts. Hydrochloric acid (1.0 M) was added to one part to adjust the pH in the acidic range. Sodium hydroxide (1.0 M) was added to the second part to adjust the pH in the basic range. The fluorescence intensity was recorded at the maximum emission wavelength every 0.2 pH interval. The pK_a value was obtained after sigmoidal fitting.

Cell incubation and fluorescence imaging: MCF-7 and HeLa cells were seeded onto cover slips at a concentration of 2×10^4 cells mL^{-1} and cultured in Dulbecco's modified Eagle medium (DMEM) in an incubator (37 °C, 5% CO_2, 20% O_2). After 24 h, the cover slips were rinsed three times with PBS to remove the media and then cultured in DMEM for later use. For the verification procedure, dyes **4** (20 μM), **5** (20 μM), **6** (20 μM), and **7** (20 μM) were added to the above cellular samples and incubated for 120 min, and **8** (5.0 μM) was incubated for 30 min; then the samples were rinsed three times with PBS and observed under an Olympus FV1000-IX81 confocal fluorescence microscope; for the confocal fluorescence imaging the 100× objective lens was used.

Fluorescent imaging in vivo: ICR mice (25 g) were given an sp (skin-pop) injection of a solution of **5** (0, 10, 20 and 50 μM in 0.1 mL of 40 mM HEPES buffer, pH 7.37). Images were taken after incubation for 10 min by using a NightOWL II LB983 small animal in vivo imaging system containing a sensitive Charge Coupled Device (CCD) camera, with an excitation filter of 630 nm and an emission filter of (655 ± 20) nm. Adult male ICR mice (25 g) were provided by the Specific Pathogen Free Animal Laboratory at Dalian Medical University. All experimental procedures were conducted in conformity with institutional guidelines for the care and use of laboratory animals in Dalian Medical University (Dalian, China) and conformed to the National Institutes of Health Guide for Care and Use of Laboratory Animals (publication no. 85–23, revised 1996).

Acknowledgements

This work was supported financially by the NSF of China (21222605, 21006009, 21136002, 2176032 and 20923006), the Fundamental Research Funds for the Central Universities of China, 973 program of China (2009CD724700 and 2012CB733702) and 863 program of China (2011AA02A105).

Keywords: colorimetric analysis · fluorescence · fluorescent probes · mitochondria · thiol probes · imaging

[1] a) X. Qian, Y. Xiao, Y. Xu, X. Guo, J. Qian, W. Zhu, *Chem. Commun.* **2010**, *46*, 6418–6436; b) A. Loudet, K. Burgess, *Chem. Rev.* **2007**, *107*, 4891–4932; c) M. S. T. Gonçalves, *Chem. Rev.* **2008**, *108*, 190–212; d) S. Hapuarachchige, G. Montao, C. Ramesh, D. Ro-

driguez, L. H. Henson, C. C. Williams, S. Kadavakkollu, D. L. Johnson, C. B. Shuster, J. B. Arterburn, *J. Am. Chem. Soc.* **2011**, *133*, 6780–6790; e) X. Peng, Z. Yang, J. Wang, J. Fan, Y. He, F. Song, B. Wang, S. Sun, J. Qu, J. Qi, M. Yan, *J. Am. Chem. Soc.* **2011**, *133*, 6626–6635; f) E. Kim, M. Koh, J. Ryu, S. B. Park, *J. Am. Chem. Soc.* **2008**, *130*, 12206–12207; g) T. Peng, D. Yang, *Org. Lett.* **2010**, *12*, 496–499; h) G. M. Fischer, C. Jungst, M. Isomaki-Krondahl, D. Gauss, H. M. Moller, E. Daltrozzo, A. Zumbusch, *Chem. Commun.* **2010**, *46*, 5289–5291.

[2] a) L. Yuan, W. Y. Lin, K. B. Zheng, L. W. He, W. M. Huang, *Chem. Soc. Rev.* **2013**, *42*, 622–661; b) K. Kiyose, H. Kojima, T. Nagano, *Chem. Asian J.* **2008**, *3*, 506–515; c) L. Yuan, W. Lin, S. Zhao, W. Gao, B. Chen, L. He, S. Zhu, *J. Am. Chem. Soc.* **2012**, *134*, 13510–13523; d) L. Yuan, W. Lin, Y. Yang, H. Chen, *J. Am. Chem. Soc.* **2012**, *134*, 1200–1211; e) G. Qian, Z. Y. Wang, *Chem. Asian J.* **2010**, *5*, 1006–1029.

[3] a) B. Tang, F. Yu, P. Li, L. Tong, X. Duan, T. Xie, X. Wang, *J. Am. Chem. Soc.* **2009**, *131*, 3016–3023; b) T. Myochin, K. Kiyose, K. Hanaoka, H. Kojima, T. Terai, T. Nagano, *J. Am. Chem. Soc.* **2011**, *133*, 3401–3409; c) Y. Lin, R. Weissleder, C.-H. Tung, *Bioconjugate Chem.* **2002**, *13*, 605–610; d) D. Oushiki, H. Kojima, T. Terai, M. Arita, K. Hanaoka, Y. Urano, T. Nagano, *J. Am. Chem. Soc.* **2010**, *132*, 2795–2801.

[4] a) Y. Koide, Y. Urano, K. Hanaoka, T. Terai, T. Nagano, *J. Am. Chem. Soc.* **2011**, *133*, 5680–5682; b) Y. Koide, Y. Urano, K. Hanaoka, W. Piao, M. Kusakabe, N. Saito, T. Terai, T. Okabe, T. Nagano, *J. Am. Chem. Soc.* **2012**, *134*, 5029–5031; c) Y. Koide, M. Kawaguchi, Y. Urano, K. Hanaoka, T. Komatsu, M. Abo, T. Terai, T. Nagano, *Chem. Commun.* **2012**, *48*, 3091–3093.

[5] a) X.-D. Jiang, R. Gao, Y. Yue, G.-T. Sun, W. Zhao, *Org. Biomol. Chem.* **2012**, *10*, 6861–6865; b) M. Nakamura, H. Tahara, K. Takahashi, T. Nagata, H. Uoyama, D. Kuzuhara, S. Mori, T. Okujima, H. Yamada, H. Uno, *Org. Biomol. Chem.* **2012**, *10*, 6840–6849.

[6] Y.-Q. Sun, J. Liu, X. Lv, Y. Liu, Y. Zhao, W. Guo, *Angew. Chem.* **2012**, *124*, 7752–7754; *Angew. Chem. Int. Ed.* **2012**, *51*, 7634–7636.

[7] T. P. Gustafson, Y. Yan, P. Newton, D. A. Hunter, S. Achilefu, W. J. Akers, S. E. Mackinnon, P. J. Johnson, M. Y. Berezin, *MedChemComm* **2012**, *3*, 685–690.

[8] E. Azuma, N. Nakamura, K. Kuramochi, T. Sasamori, N. Tokitoh, I. Sagami, K. Tsubaki, *J. Org. Chem.* **2012**, *77*, 3492–3500.

[9] X. Xiong, F. Song, S. Sun, J. Fan, X. Peng, *Asian J. Org. Chem.* **2013**, *2*, 145–149.

[10] B. A. Sparano, K. Koide, *J. Am. Chem. Soc.* **2007**, *129*, 4785–4794.

[11] a) H. Maeda, Y. Futkuyasu, S. Yoshida, M. Fukuda, K. Saeki, H. Matsuno, Y. Yamauchi, K. Yoshida, K. Hirata, K. Miyamoto, *Angew. Chem.* **2004**, *116*, 2443–2445; *Angew. Chem. Int. Ed.* **2004**, *43*, 2389–2391; b) B. C. Dickinson, C. Huynh, C. J. Chang, *J. Am. Chem. Soc.* **2010**, *132*, 5906–5915; c) E. W. Miller, O. Tulyanthan, E. Y. Isacoff, C. J. Chang, *Nat. Chem. Biol.* **2007**, *3*, 263–267; d) E. W. Miller, O. Tulyathan, E. Y. Isacoff, C. J. Chang, *Nat. Chem. Biol.* **2007**, *3*, 349–349; e) B. Heyne, V. Maurel, J. C. Scaiano, *Org. Biomol. Chem.* **2006**, *4*, 802–807.

[12] D. Yang, H. L. Wang, Z. N. Sun, N. W. Chung, J. G. Shen, *J. Am. Chem. Soc.* **2006**, *128*, 6004–6005.

[13] a) F. He, Y. L. Tang, M. H. Yu, S. Wang, Y. L. Li, D. B. Zhu, *Adv. Funct. Mater.* **2006**, *16*, 91–94; b) K. H. Xu, X. Liu, B. Tang, *ChemBioChem* **2007**, *8*, 453–458; c) H. Maeda, K. Yamamoto, I. Kohno, L. Hafsi, N. Itoh, S. Nakagawa, N. Kanagawa, K. Suzuki, T. Uno, *Chem. Eur. J.* **2007**, *13*, 1946–1954; d) K. H. Xu, X. Liu, B. Tang, G. W. Yang, Y. Yang, L. G. An, *Chem. Eur. J.* **2007**, *13*, 1411–1416; e) H. Maeda, K. Yamamoto, Y. Nomura, I. Kohno, L. Hafsi, N. Ueda, S. Yoshida, M. Fukuda, Y. Fukuyasu, Y. Yamauchi, N. Itoh, *J. Am. Chem. Soc.* **2005**, *127*, 68–69.

[14] a) H. Wang, G. Zhou, H. Gai, X. Chen, *Chem. Commun.* **2012**, *48*, 8341–8343; b) X. Chen, S. K. Ko, M. J. Kim, I. Shin, J. Yoon, *Chem. Commun.* **2010**, *46*, 2751–2753; c) H. Wang, G. Zhou, C. Mao, X. Chen, *Dyes Pigm.* **2013**, *96*, 232–236; d) H. Wang, G. Zhou, X. Chen, *Sensor. Actuat. B-Chem.* **2013**, *176*, 698–703; e) H. Maeda, H. Matsuno, M. Ushida, K. Katayama, K. Saeki, N. Itoh, *Angew. Chem.* **2005**, *117*, 2982–2985; *Angew. Chem. Int. Ed.* **2005**, *44*, 2922–2925; f) O. Rusin, N. N. St. Luce, R. A. Agbaria, J. O. Escobedo, S. Jiang, I. M. Warner, F. B. Dawan, K. Lian, R. M. Strongin, *J. Am. Chem. Soc.* **2004**, *126*, 438–439.

[15] M. R. Wasielewski, D. G. Johnson, M. P. Niemczyk, G. L. Gaines, M. P. O'Neil, W. A. Svec, *J. Am. Chem. Soc.* **1990**, *112*, 6482–6488.

[16] J. S. Lee, Y. K. Kim, M. Vendrell, Y. T. Chang, *Mol. BioSyst.* **2009**, *5*, 411–421.

[17] a) A. T. Hoye, J. E. Davoren, P. Wipf, M. P. Fink, V. E. Kagan, *Acc. Chem. Res.* **2008**, *41*, 87–97; b) L. F. Yousif, K. M. Stewart, S. O. Kelley, *ChemBioChem* **2009**, *10*, 1939–1950; c) J. Nunnari, A. Suomalainen, *Cell* **2012**, *148*, 1145–1159; d) J. Bereiter-Hahn, M. Voth, S. Mai, M. Jendrach, *Biotechnol. J.* **2008**, *3*, 765–780; e) S. Zhang, T. Wu, J. L. Fan, Z. Y. Li, N. Jiang, J. Y. Wang, B. R. Dou, S. G. Sun, F. L. Song, X. J. Peng, *Org. Biomol. Chem.* **2013**, *11*, 555–558.

[18] F. Rashid, R. W. Horobin, *J. Microsc.* **1991**, *163*, 233–241.

[19] H. Zhu, J. L. Fan, Q. L. Xu, H. L. Li, J. Y. Wang, P. Gao, X. J. Peng, *Chem. Commun.* **2012**, *48*, 11766–11768.

[20] A. Roos, W. F. Boron, *Physiol. Rev.* **1981**, *61*, 296–433.

[21] E. P. Serjeant, B. Dempsey, *Biochim. Biophys. Acta* **1979**, *977*, 266–277.

[22] J. C. Castro, A. Malakhov, K. Burgess, *Synthesis* **2009**, *7*, 1224–1226.

Received: February 2, 2013
Published online: ■■ ▮▮, 0000

Born to dye: Five fluorescein analogues were synthesised (see scheme). One analogue was found to emit in the NIR region with a high quantum yield, excellent photostability and good permeability. Three derivatives were found to specifically stain mitochondria and one dye responds to thiols with a strong turn-on NIR fluorescence signal and colorimetric change, in vitro and in vivo.

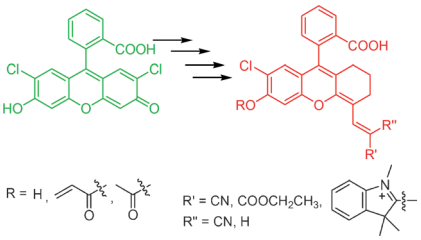

Fluorescent Probes

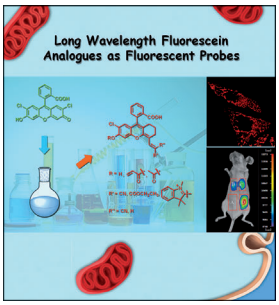

Long Wavelength Fluorophores

Biological imaging in the red and near-infrared (NIR) region is desirable due to its deep tissue penetration and minimum background autofluorescence from biomolecules in living systems. However, photostable NIR small-molecule fluorophores are limited. In their Communication on page ■■ ff., X. Xiong et al. report five photostable fluorescein analogues obtained through a Vilsmeier reaction and Knoevenagel condensation. The new NIR fluorophores retain the particular characteristics of fluoresceins, but exhibit excellent bioimaging capabilities in both living cells and mice.